Applied Catalysis B: Environmental 217 (2017) 100–107

Contents lists available at ScienceDirect

Applied Catalysis B: Environmental

journal homepage: www.elsevier.com/locate/apcatb

CdS/Pt photocatalytic activity boosted by high-energetic photons based on efficient triplet–triplet annihilation upconversion

Jiaojiao Fang[a,c], Wei Wang[b,c,*], Cheng Zhu[a,c], Liang Fang[a,c], Junyang Jin[a,c], Yaru Ni[a,c], Chunhua Lu[a,c,*], Zhongzi Xu[a,c]

[a] State Key Laboratory of Materials-Orient Chemical Engineering, College of Materials Science and Engineering, Nanjing Tech University, Nanjing 210009, PR China
[b] School of Physics and Optoelectronic Engineering, Nanjing University of Information Science & Technology, Nanjing 210044, PR China
[c] Jiangsu Collaborative Innovation Center for Advanced Inorganic Function Composites, Nanjing Tech University, Nanjing 210009, PR China

ARTICLE INFO

Article history:
Received 27 March 2017
Received in revised form 19 May 2017
Accepted 22 May 2017
Available online 27 May 2017

Keywords:
Triplet–triplet annihilation
Upconversion
Photocatalysis
High energy photons

ABSTRACT

We herein report the triplet–triplet annihilation upconversion luminescence (TTA-UCL) clusters achieved by loading the platinum(II)-octaethylporphyrin (PtOEP) and 9,10-diphenylanthracene (DPA) into silica shells. This aqueous-based system possesses a core–shell structure which is of crucial importance for enhancing the mobility of core liquid. The encapsulated clusters with efficient green-to-blue upconversion without deoxygenation are conjoined with cadmium sulfide (CdS) as the photocatalyst. Platinum (Pt) is used to improve the separation of electron−hole pairs on the photocatalytic system. Given the band gap of photocatalysts, tetracycline (TC) degradation and photoinduced hydrogen evolution are used to perform the photocatalytic activity. CdS loaded with Pt has higher Pseudo-first-order rate constant (k_{pfo}) in decomposing tetracycline than pure CdS. Moreover, the excellent hydrogen evolution property appears when the converted high energy photons from TTA-UCL-based clusters are introduced to the photocatalytic system. The quantum efficiency of hydrogen evolution increases further after the cocatalyst Pt deposition. This work not only fabricates an encapsulated structure for TTA-UCL clusters, but also provides an effective TTA-supported upconversion-photocatalysis system.

1. Introduction

Photocatalysis technology is considered as one of the most promising approaches for making use of sunlight to degrade toxic and harmful substances [1,2]. Key factors to promote the photocatalytic efficiency include realization of broad-band absorption, utilization of the sunlight and efficient separation of photogenerated electron-hole pairs [3,4]. Recently, enhancing photocatalytic activity by high energy photons is becoming a new research direction in this field [5–7]. Nevertheless, high energy photons occupy only a small proportion of the sunlight energy compared to lower energy photons.

Upconversion, which is the anti-stokes shift process of absorbing lower energy photons and emitting higher energy photons [8–10], has the potential to broaden the available solar spectrum range and raise the proportion of higher energy photons. To date, there are several reports about lanthanide based upconversion materials applying in the photocatalytic field [11–13]. However, traditional rare earth upconversion materials have weak absorption cross section, high excitation threshold, and poor overall upconversion capability, etc. [14–16]. In contrast, triplet–triplet annihilation upconversion luminescence (TTA-UCL) as a new alternative upconversion approach has attracted more and more attention, due to its low excitation power density with noncoherent sunlight, high upconversion quantum yield and broad absorption spectra [17–19]. So far, TTA-UCL has been applied mainly for organic light-emitting diodes [20–22] and bioimaging [23–25]. Rare literatures about TTA-UCL combing with photocatalysts have been reported [26–28]. Recent researches on TTA-UCL are based on nonpolar organic solvents avoiding oxygen quenching [29–31]. It is still a challenge for realizing efficient TTA-UCL in aqueous environments, which can be applied in the photocatalytic field. Moreover, maintenance of high mobility of sensitizers and emitters is of great importance for efficient energy transfer processes [26]. It has been reported that encapsulating sensitizers and emitters in inert matrices and constructing a core-shell structure, such as micelles [32,33], capsules [34,35,23], and nanoparticles [24,26,29], offer an alternative

* Corresponding authors at: Jiangsu Collaborative Innovation Center for Advanced Inorganic Function Composites, Nanjing Tech University, Nanjing 210009, PR China.
E-mail addresses: wwang@nuist.edu.cn (W. Wang), chhlu@njtech.edu.cn (C. Lu).

http://dx.doi.org/10.1016/j.apcatb.2017.05.069
0926-3373/

to achieve the high TTA-UCL efficiency. Such procedure could also be helpful for TTA-UCL-based materials to couple with the semiconductor photocatalysts, which is expected to improve the photocatalytic activity compared to simple physical blending [28].

Herein, we present a core–shell structure to encapsulate the inert organic medium containing TTA chromophores (PtOEP as the sensitizer and DPA as the emitter) in a rigid silica shell which provides a solid and hydrophilic surface for CdS deposition. To further boost the photocatalytic efficiency, the noble metal Pt as co-catalyst is deposited on CdS surface to facilitate the separation of photo-generated electrons and holes. The morphology, crystallographic phase and elemental analysis of upconversion-photocatalytic composites are examined. The absorption spectra, fluorescence property as well as photocatalytic performance are discussed subsequently. The synthesized samples are expected to exhibit a superior photocatalytic degradation capacity for TC and the hydrogen evolution property based on the TTA-UCL process when they are exposed to a specific waveband light.

2. Experimental

2.1. Materials

Analytical grade tetrahydrofuran (THF, >99%, Sinopharm Chemical Reagent Co., Ltd.), ethyl silicate (TEOS, Sinopharm Chemical Reagent Co., Ltd.), cadmium chloride ($CdCl_2$, >99.0%, Sinopharm Chemical Reagent Co., Ltd.), thioacetamide (>99.0%, Shanghai LinFeng Chemical Reagent Co., Ltd.), chloroplatinic acid ($H_2PtCl_6 \cdot 6H_2O$, Sinopharm Chemical Reagent Co., Ltd.) triethanolamine (TEA, Shanghai LinFeng Chemical Reagent Co., Ltd.), tetracycline (TC, Shanghai Macklin Biochemical Co., Ltd.) and methanol (>99.5%, WuXi City YaSheng Chemical Co., Ltd.) were used without further purification. Oleic acid (OA, 97%), 9,10-diphenylanthracene (DPA, 97%) and (3-Aminopropyl)- trimethoxysilane (APTMS, 97%) were all purchased from Aldrich. Moreover, platinum (II)-octaethylporphyrin (PtOEP) were purchased from Frontier Scientific and used as received. The 10 mg of PtOEP and 13 mg of DPA in THF were separately prepared and stored in the dark. The OA solution was prepared by adding PtOEP solution (2.5 mL, 1 mmol/L) and DPA solution (3 mL, 2 mmol/L) into 5 mL OA. The solution was placed in an oven at 70 °C for 12 h to completely evaporate the THF, and then cooled to room temperature naturally.

2.2. Preparation of silica nanoparticles composed of PtOEP&DPA

The preparation of PtOEP&DPA-containing silica (PtDPA@SiO_2) nanoparticles followed a previously reported method with a few modifications [26]. The OA mixture (300 μL) with PtOEP&DPA (PtDPA) was mixed with deionized water (100 mL) and sonicated for emulsification. Given such vigorous stirring, 1 mmol of APTMS was added dropwise to the emulsion to obtain a kind of approximatively transparent bright pink solution. Whereafter, 6 mmol of TEOS was injected into the mentioned solution and the mixture color was gradually transformed to white. The resulting mixture was gently stirred (100–150 r/min) at 55 °C for 48 h. After reaction, the precipitate was centrifuged and washed with deionized water. Finally, the sample was dried in a vacuum oven at 70 °C for 12 h.

The sample OA@SiO_2 was prepared by using the isovolumetric OA to substitute for the OA-PtDPA mixture and other experimental procedures were the same.

2.3. PtDPA@SiO_2 and OA@SiO_2 deposited with CdS nanoparticles

PtDPA@SiO_2 or OA@SiO_2 (0.1 g) was dispersed in 30 mL of ethanol, respectively. APTMS (0.7 mL) was then added into the mixture at ambient temperature and the whole suspension was under magnetic stirring (150 rpm) for 12 h. After washing with deionized water, the obtained nanoparticles modified with amino groups were treated with $CdCl_2$ aqueous solution (20 mL, 0.1 mmol/L) and then stirred for 4 h. The precipitate was further dispersed to 20 mL thioacetamide aqueous solution (0.1 mmol/L) under stirring at 100 °C for 24 h. The final products were separately denoted as PtDPA@SiO_2@CdS and OA@SiO_2@CdS.

2.4. Photo-deposition of Pt nanoparticles

PtDPA@SiO_2@CdS (20 mg) was dispersed in 100 mL deionized water, followed by adding the methanol (100 μL) and H_2PtCl_6 aqueous solution (100 μL, 25 mmol/L) successively. The mixture was irradiated with a 365 nm LED for 2 h and the products with Pt deposition (PtDPA@SiO_2@CdS/Pt) were obtained.

2.5. Characterizations

The crystal structure was measured with the X-ray diffractometer (XRD, SmartLab-3KW, Rigaku, Japan), using Cu Kα radiation (λ = 0.15406 nm) at the scanning speed of 10°/min. The absorption spectra were analyzed on an UV-vis-NIR spectrophotometer (UV3101PC, Shimadzu Corp., Japan). Field emission scanning electron microscope (FESEM, SU8010, Hitachi, Japan) was used to analyse the morphology of as-obtained samples. Transmission electron microscopy (TEM) analysis was conducted on the electron microscope (JEOL JEM-2100, Japan). The fluorescence spectra were collected through the fluorescence spectrophotometer (Jobin Yvon FL3-221, HORIBA, France). The hydrogen gas quantity was analyzed by the gas chromatography system (Agilent Technologies 7890B, America).

2.6. Photocatalytic activity experiments

TC as a typical antibiotic was selected to test the photocatalytic activities of the prepared samples under xenon lamp radiation with a 520 nm hand-pass optical filter/cut-off filter (780 nm > λ > 400 nm). The sample (0.1 g) was dispersed in 100 mL TC aqueous solution (20 mg/L) and then the dispersion was stirred in the dark for 1 h to reach the absorption–desorption equilibrium. 4 mL suspensions were collected at a certain irradiation time interval (10 min) and the supernatant was extracted by centrifugation. The absorbance of the tetracycline aqueous solution at 360 nm was gauged by the UV–vis-NIR spectrophotometer.

The photocatalytic hydrogen evolution reaction was carried out in a quartz flash with the base area of 19.75 cm^2. The photocatalyst (50 mg) was dispersed in 40 mL aqueous solution containing 10% TEA as sacrificial reagents. The suspension was irradiated after bubbling argon into the solution for 30 min by a xenon lamp (300W) with a 520 nm hand-pass optical filter/cut-off filter (780 nm > λ > 400 nm). The gas produced was analyzed using the gas chromatography system equipped with a 5 mL syringe.

3. Results and discussion

Scheme 1 illustrates the established procedure for TTA-UCL clusters fabrication. For isolating oxygen and keeping PtDPA chromophores' liquidity, the emulsion process for preliminarily encapsulating PtDPA chromophores was used [26]. Then TEOS is hydrated to produce the rigid shell for subsequent CdS deposition. The as-obtained product finally deals with Pt modification by the photochemical deposition method.

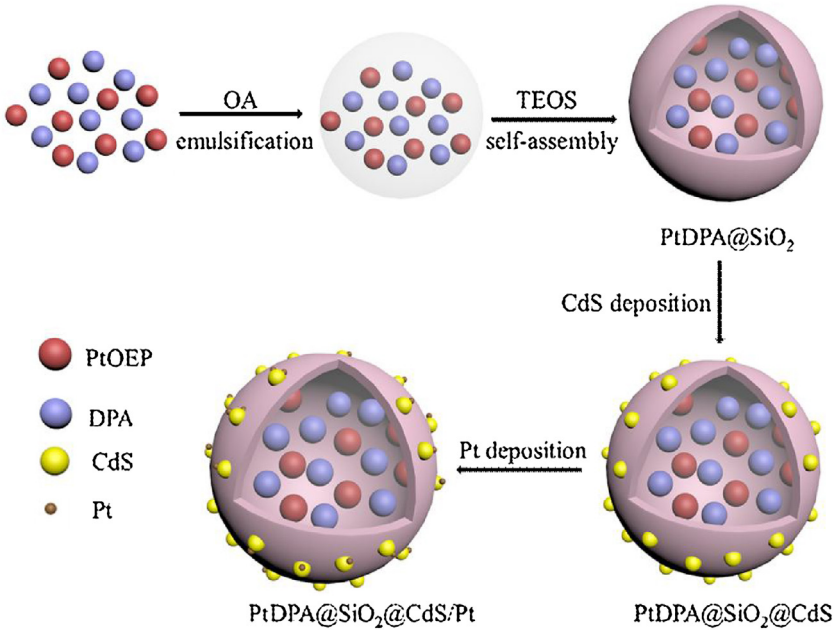

Scheme 1. Schematic illustration of TTA-UCL clusters fabrication process.

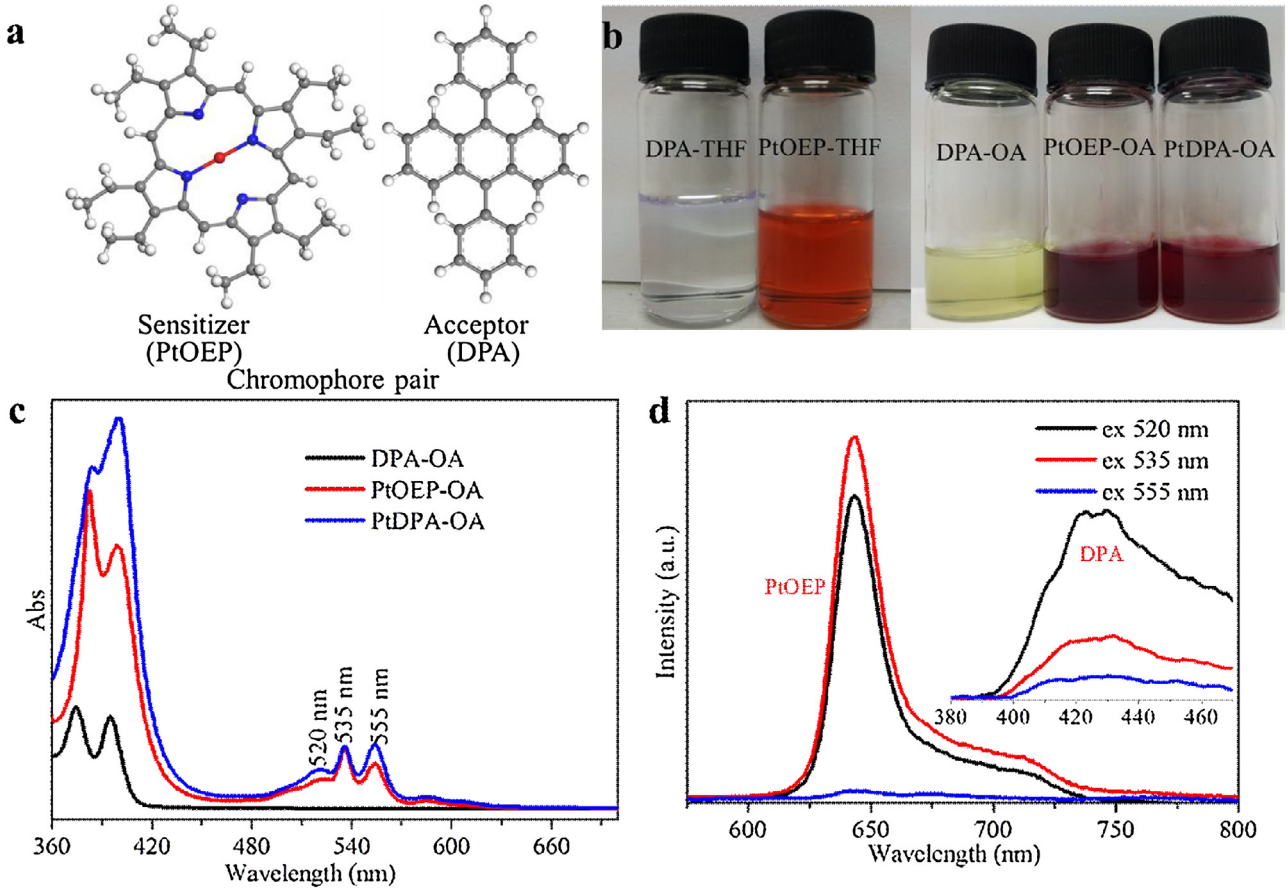

Fig. 1. (a) The ball-stick geometric structures of PtOEP and DPA chromophore pair, −Pt–N–C–H. (b) The photographs of PtOEP, DPA and PtDPA in THF and OA, respectively. (c) The absorption spectra of PtOEP, DPA and PtDPA separately dispersed in OA. (d) The emission spectra of PtDPA in OA under xenon lamp radiation with different excitation wavelengths.

3.1. Introduction of the chromophores solution

The chemical structures of PtOEP and DPA are shown in Fig. 1a. The complex PtOEP with phosphorescence maxima at ~650 nm (>1.90 eV) is used as the sensitizer, and triplet state energy of DPA is 1.77 eV [36,17], which meets the requirement of E_{T1}(sensitizer) > E_{T1}(acceptor). Hence, DPA can be used to match with PtOEP for TTA-UCL. The chromophores dissolved in THF or

Fig. 2. Photograph of the samples OA@SiO_2, PtDPA@SiO_2, PtDPA@SiO_2@CdS and PtDPA@SiO_2@CdS/Pt.

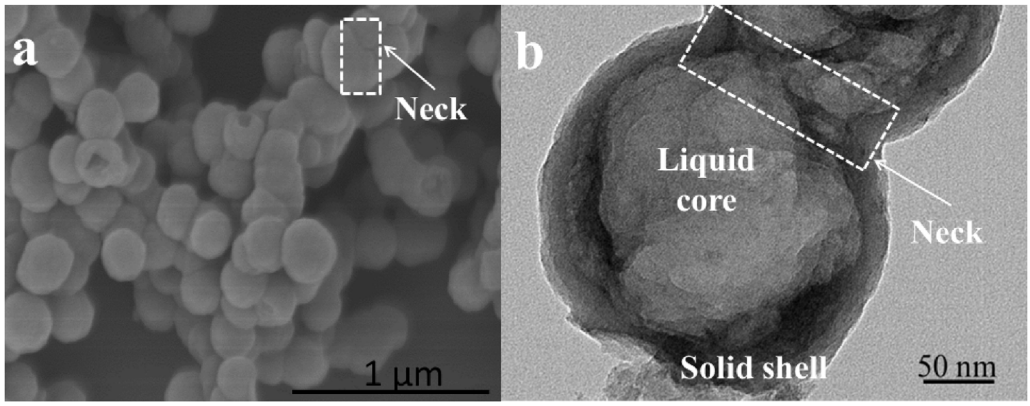

Fig. 3. (a) FESEM image and (b) TEM image of the synthesized PtDPA@SiO_2.

OA are transparent (Fig. 1b). OA with unsaturated double bonds can capture electrons from singlet oxygen. Accordingly, it can be chosen as the optimal solvent to dissolve PtDPA chromophores. The absorption spectra in Fig. 1c display intense absorption bands of PtOEP in OA (at 360–450 nm) and the characteristic absorption bands at 520, 535 and 555 nm, respectively, while DPA dissolved in OA only shows weak absorption bands at 360–420 nm. Under xenon lamp radiation separately at 520, 535 and 555 nm, PtDPA in OA shows the upconversion luminescence at 400–440 nm and the luminescent intensity is enhanced as the incident light power increases (Fig. 1d). In addition, the phosphorescence peak around 643 nm is ascribed to the Stokes emission from triplet state of PtOEP and the phosphorescence intensity is relatively reductive with triplet–triplet energy transfer process.

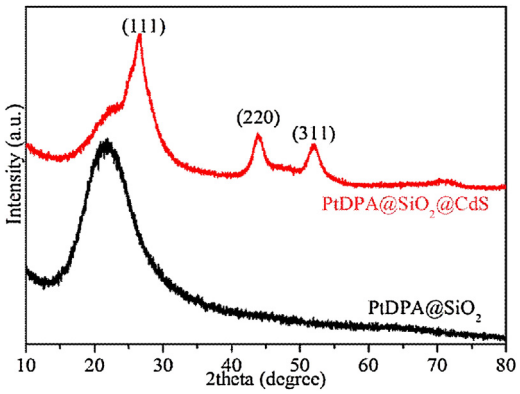

Fig. 4. XRD spectra of PtDPA@SiO_2 and PtDPA@SiO_2@CdS samples.

3.2. Structural characterization of TTA-UCL clusters

The synthetic samples are shown in Fig. 2. OA@SiO_2 nanoparticles are faint yellow. After the deposition of CdS, the color of PtDPA@SiO_2 clusters is transformed from pale pink to golden yellow. PtDPA@SiO_2@CdS/Pt becomes dark brown on account of loading Pt nanoparticles. The morphology of the synthesized PtDPA@SiO_2 is shown in Fig. 3a. The particle diameter approaches to 200 nm. Meanwhile, the neck structure between particles (Fig. 3b) may act as bridge which increases the local mobility of liquid core coated by solid shells. Hence, this special structure could be in favour of improving luminous efficacy.

Compared to PtDPA@SiO_2 clusters, the XRD pattern of PtDPA@SiO_2@CdS shows the favorable crystallographic phase of CdS nanoparticles (Fig. 4). The diffraction peaks located at 26.5°, 43.9° and 52.1° correspond to the (111), (220) and (311) planes of the CdS [37], respectively.

To illustrate the distribution of CdS particles loaded on the surface of as-obtained PtDPA@SiO_2, the SEM image from Fig. 5a shows that lots of small CdS particles with diameter of 10 nm are attached on the PtDPA@SiO_2@CdS surface. The result also is presented in Fig. 5b which indicates the combination of the solid shells of PtDPA@SiO_2 clusters and CdS particles. To further verify the interaction between PtDPA@SiO_2 and CdS nanoparticles, the characteristic wrinkle is analyzed by the HRTEM. As shown in Fig. 5c, the lattice fringes of CdS nanoparticles are fairly apparent. The planar spacings are 0.36 nm and 0.336 nm, which can be corresponding to the (100) and (111) planes of CdS, respectively [37–39]. Even though there are many small nanoparticles linked to PtDPA@SiO_2@CdS/Pt (Fig. 5d), the photodeposition of Pt nanoparticles onto the surface of PtDPA@SiO_2@CdS can't be analysed from Fig. 5d and e directly, since the particle diameter of Pt is far less than CdS nanoparticles. Fig. 5f shows that Pt has the particle diameter

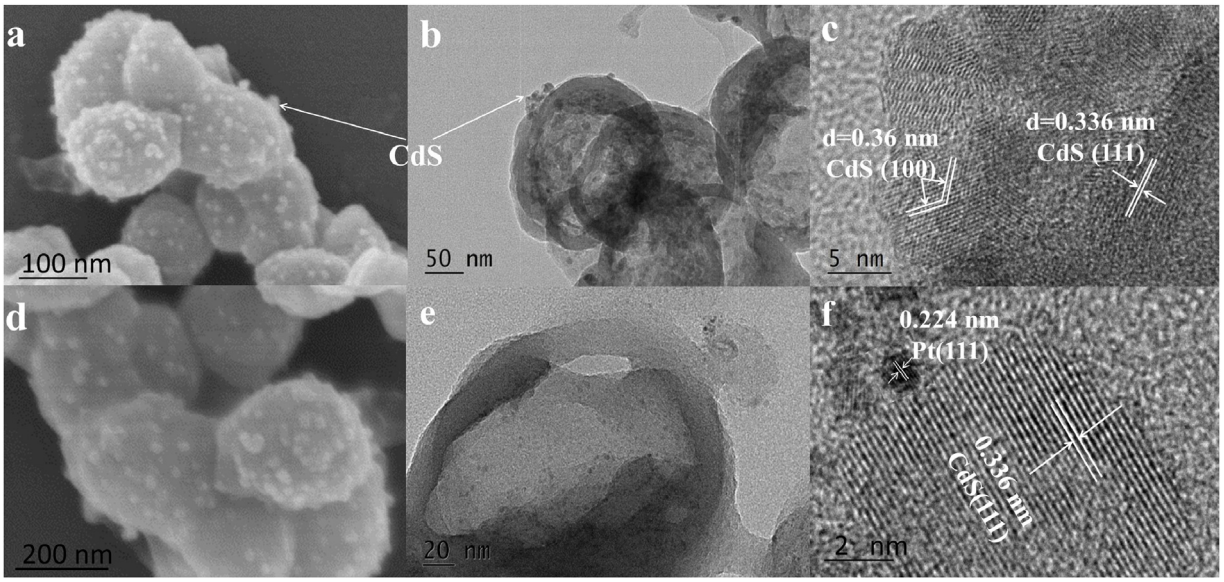

Fig. 5. (a) SEM image, (b) TEM image and (c) HRTEM image of PtDPA@SiO_2@CdS clusters. (d) SEM image, (e) TEM image and (f) HRTEM image of PtDPA@SiO_2@CdS/Pt.

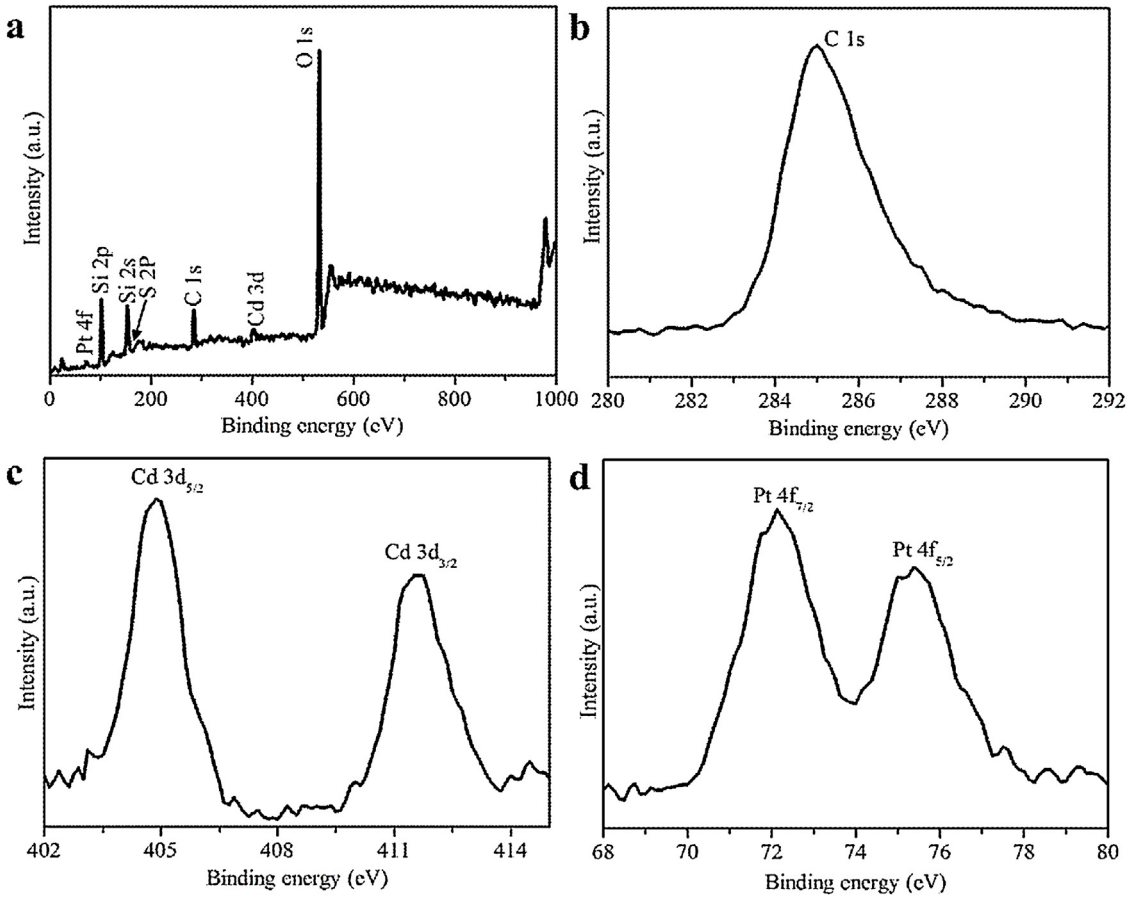

Fig. 6. (a) XPS spectra of PtDPA@SiO_2@CdS/Pt nanoparticles, XPS spectra of (b) C 1s, (c) Cd 3d and (d) Pt 4f from PtDPA@SiO_2@CdS/Pt nanoparticles.

of 1 nm approximately and the crystalline interplanar spacings of PtDPA@SiO_2@CdS/Pt are 0.224 nm and 0.336 nm, which are separately assigned to the (111) planes of Pt and CdS [40,38]. The analysis mentioned indicates that CdS links to PtDPA@SiO_2 clusters and Pt is connected firmly in PtDPA@SiO_2@CdS/Pt.

The XPS spectra of PtDPA@SiO_2@CdS/Pt nanoparticles shown in Fig. 6a are employed to further confirm that CdS and Pt are deposited successfully and the chromophores (PtDPA) are entirely wrapped into SiO_2 particles. The peaks of Pt 4f, Si 2p, Si 2s, C 1s and O 1s are collected from PtDPA@SiO_2@CdS/Pt clusters. The C 1s peak without other impure peaks (Fig. 6b) can be considered from the results of the adhesive carbon families [26]. There is no existence of N1s around 400 eV (Fig. S1 and Fig. S3), at the same time, it's no exhibition of Pt elements in the XPS spectra of PtDPA@SiO_2@CdS (Fig.

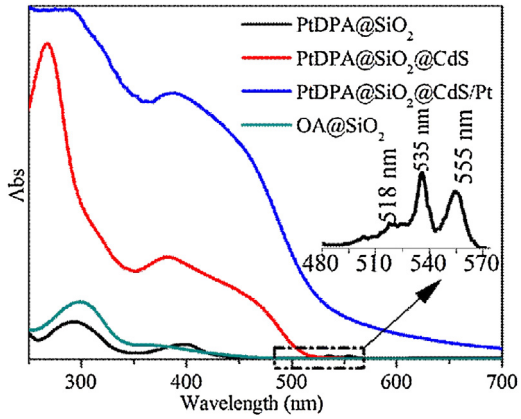

Fig. 7. Absorption spectra of the samples $OA@SiO_2$, $PtDPA@SiO_2$, $PtDPA@SiO_2@CdS$ and $PtDPA@SiO_2@CdS/Pt$.

S2 and Fig. S4), suggesting that all chromophores are only encapsulated in the SiO_2 shells. Besides, the existence of Cd 3d peaks (Fig. 6c) and Pt 4f peaks (Fig. 6d) can verify that CdS and Pt are successfully deposited on the surface of $PtDPA@SiO_2$, respectively.

3.3. Properties of TTA-UCL clusters

By analyzing the absorption spectra in Fig. 7, $PtDPA@SiO_2$ clusters shows the characteristic absorption bands at 518, 535 and 555 nm, which are in agreement with the absorption bands of PtDPA dissolved OA (Fig. 1c). Thus, the encapsulation of SiO_2 has no effect on the absorption peak position of the chromophores. Comparing with $PtDPA@SiO_2$ clusters, the sample $PtDPA@SiO_2@CdS$ has the absorption band side at 510 nm. Deposition with Pt nanoparticles enhances further the whole absorption intensity significantly, which could attribute to the depressed reflectivity by the dark brown color of $PtDPA@SiO_2@CdS/Pt$ and the size effect of Pt nanoparticles over the surface of $PtDPA@SiO_2@CdS$. The capacity of light absorption changes with the size and amount of Pt nanoparticles [41,42]. The absorption edge of $PtDPA@SiO_2@CdS/Pt$ broadens to 544 nm which could be due to the modified chemical and electronic properties after the presence of noble metal on the surfaces [43].

Upon excitation at different wavelengths, the sample $PtDPA@SiO_2$ displays effectively green-to-blue upconversion luminescence and the luminescent intensity increases with decreasing excitation wavelength (Fig. 8a). And yet, Fig. 8b shows no emission peak for $PtDPA@SiO_2@CdS$ and $PtDPA@SiO_2@CdS/Pt$ irradiated by the xenon lamp as a function of 520 nm incident power. This is mainly considered that the samples $PtDPA@SiO_2@CdS$ and $PtDPA@SiO_2@CdS/Pt$ absorb the blue upconversion luminescence from $PtDPA@SiO_2$ clusters under excitation at 520 nm.

The green excited light with lower energy photons ($2.23\,eV < E < 2.38\,eV$) can't acitve the catalyst CdS that has a band-gap width of 2.4 eV, while obtained higher energy photons ($3.06\,eV > E > 2.91\,eV$) through TTA-UCL process can sensitize effectively CdS. The Fermi level of noble metal Pt (at −5.65 eV) is lower than the conduction band of CdS (The conduction band position of CdS with respect to the Fermi-level locates at −4.4 eV [44]). The sensitized CdS further makes the photogenerated electrons transfer to the noble metal Pt (Scheme 2). The Schottky barrier between

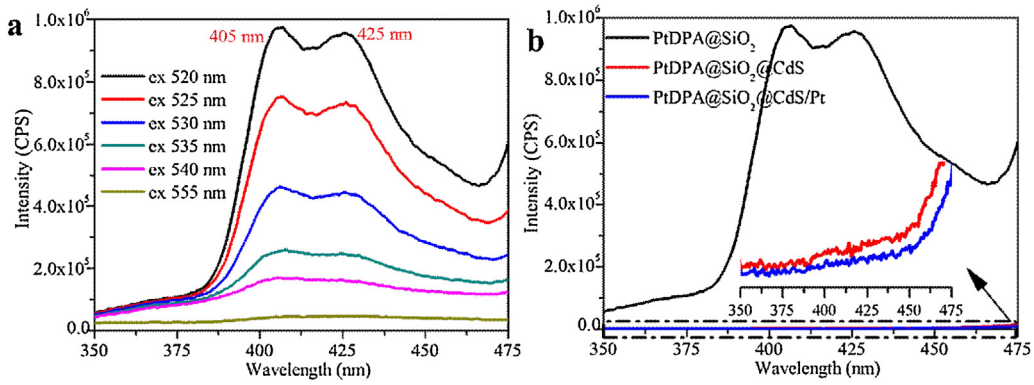

Fig. 8. (a) Fluorescence emission spectra of $PtDPA@SiO_2$ clusters under the xenon lamp radiation with different excitation intensity and (b) fluorescence emission spectra of $PtDPA@SiO_2$, $PtDPA@SiO_2@CdS$ and $PtDPA@SiO_2@CdS/Pt$ with the xenon lamp radiation (λ_{ex} = 520 nm).

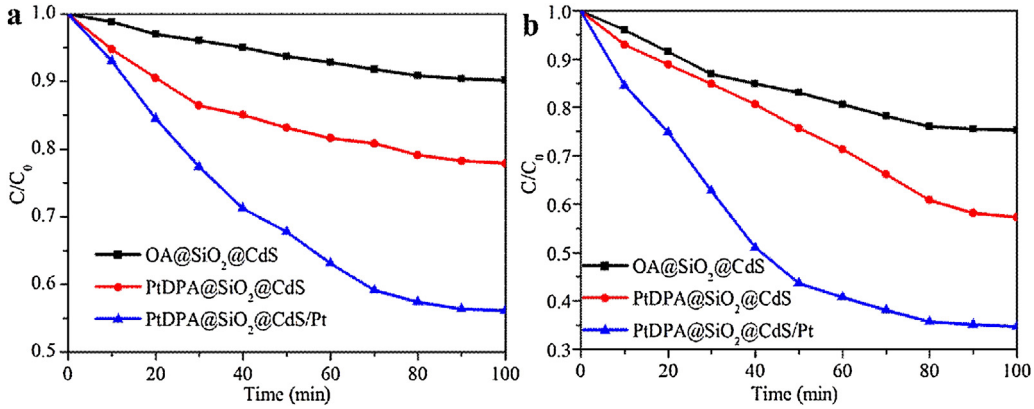

Fig. 9. (a) Under the xenon lamp radiation with a 520 nm hand-pass optical filter and (b) under the visible light irradiation, photocatalytic degradation of TC over the samples $OA@SiO_2@CdS$, $PtDPA@SiO_2@CdS$ and $PtDPA@SiO_2@CdS/Pt$.

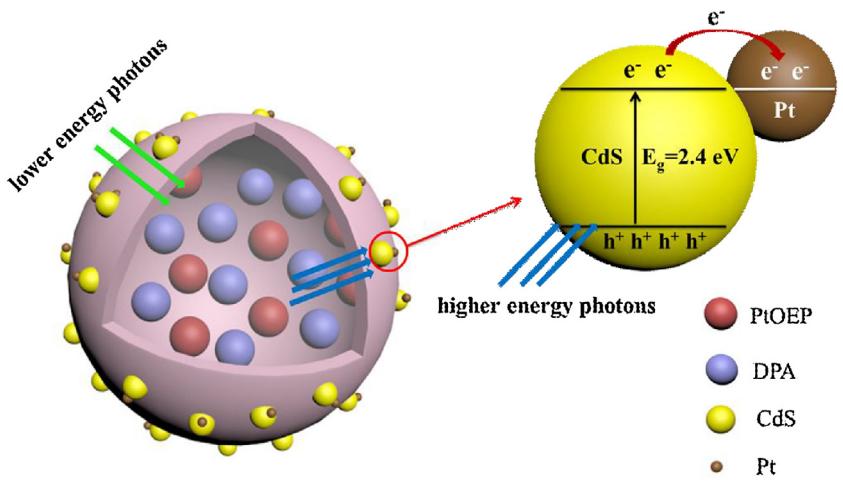

Scheme 2. Schematic illustration of the photocatalysis mechanism of PtDPA@SiO_2@CdS/Pt based on TTA-UCL process.

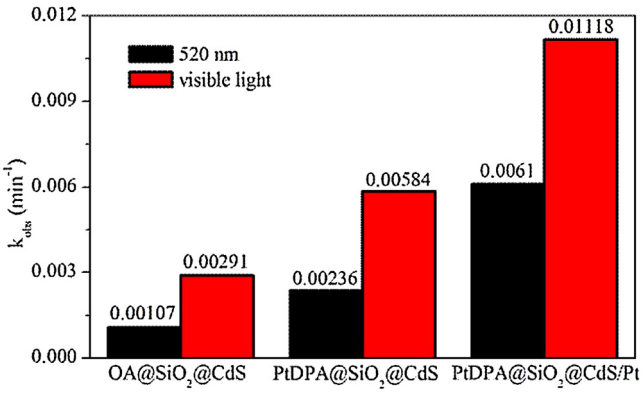

Fig. 10. Pseudo-first-order rate constant (k_{pfo}) of degrading TC with the photocatalysts under different light irradiation.

Pt and CdS can suppress the reverse migration of electrons and enhance the separation of electron–hole pairs generated from the band gap photoexcitation that can improve photocatalytic activity effectively [45]. TC as one kind of emerging pollutant is chosen to verify the excellent photocatalytic activity of PtDPA@SiO_2@CdS/Pt. Fig. 9a shows the photocatalytic degradation efficiency for TC under xenon lamp radiation with a 520 nm hand-pass optical filter that has an intensity transmission around the wavelength of 520–540 nm (Fig. S6). Besides, the Pseudo-first-order degradation kinetics and reaction rate constant (k_{pfo}) of TC with the photocatalysts are shown in Fig. S5 and Fig. 10. OA@SiO_2@CdS gives inferior degradation ability (k_{pfo} 0.00107) because of its weak absorption of the transmissible light from the optical filter and there is no light conversion performance. While PtDPA@SiO_2@CdS clusters displays higher degradation efficiency and the k_{pfo} (0.00236) increases by 1.21 fold, because it can absorb the transmissible light and the obtained high energy photons based on TTA-UCL can improve separation of electron-hole pairs to a great extent. The degradation quantity of PtDPA@SiO_2@CdS/Pt (k_{pfo} 0.0061) on the TC reaches upwards of 44% in 100 min (Fig. 9a), indicating that the noble metal Pt is beneficial to promoting the photocatalytic activity. Under visible light irradiation, the photocatalytic degradation quantities of OA@SiO_2@CdS, PtDPA@SiO_2@CdS and PtDPA@SiO_2@CdS/Pt on tetracycline are 25%, 43% and 66% in the same 100 min, respectively (Fig. 9b). The k_{pfo} of PtDPA@SiO_2@CdS/Pt (0.01118) under visible light irradiation is 3.84 fold of that using OA@SiO_2@CdS (0.00291) and 1.91 fold of that using PtDPA@SiO_2@CdS (0.00584) (Fig. 10).

Table 1
The quantum efficiency and the rate of hydrogen evolution of OA@SiO_2@CdS, PtDPA@SiO_2@CdS and PtDPA@SiO_2@CdS/Pt.

Irradiation	Visible light		The xenon lamp with a 520 nm hand-pass optical filter	
Samples	K (μmol/h)	Φ	K (μmol/h)	Φ
OA@SiO_2@CdS	8.8262	0.0175%	–	–
PtDPA@SiO_2@CdS	17.1695	0.0341%	0.2148	0.0435%
PtDPA@SiO_2@CdS/Pt	22.7966	0.0453%	0.3839	0.0777%

These catalytic performances indicate that Pt realizes the effective separation of photogenerated carriers.

The evolved hydrogen amount from as-prepared photocatalysts is studied in 40 mL aqueous solution containing 10% TEA as sacrificial reagents. As shown in Fig. 11, PtDPA@SiO_2@CdS exhibits enhanced photocatalytic hydrogen production in comparison with OA@SiO_2@CdS under visible light irradiation, while the utmost evolution of hydrogen (130 μmol) is observed over PtDPA@SiO_2@CdS/Pt due to an introduction of the local electric field from the noble metal potentially. The quantum efficiency (Φ) and the rate (K) of hydrogen evolution are summarized in Table 1. The enhanced quantum efficiency of hydrogen evolution over PtDPA@SiO_2@CdS (Φ 0.0341%) under visible light compared with OA@SiO_2@CdS (Φ 0.0175%) can be attributed to TTA-UCL induced activity. Under the xenon lamp with a 520 nm hand-pass optical filter, the optimal Φ (0.0777%) is obtained using PtDPA@SiO_2@CdS/Pt with the cocatalyst Pt deposition. Compared with OA@SiO_2@CdS that has few hydrogen productions, the Φ of PtDPA@SiO_2@CdS attaches to 0.0435%, which can be resulted from the effective sensitization from obtained high energy photons based on TTA-UCL process.

4. Conclusions

In summary, we have reported an encapsulated core-shell structure for PtOEP&DPA chromophores to enhance the mobility of the core liquid, and made a systematic study on enhancing the photoreaction activity of TTA-UCL clusters by surface functionalization. After CdS loading, the clusters achieved high energetic photons-driven photocatalysis by TTA-UCL process and the separation of photogenerated electron–hole pairs is faster over the Pt further modified photocatalysts. The degradation of TC was used to measure the photocatalytic activity and PtDPA@SiO_2@CdS/Pt displayed highest photodegradation efficiency in our research. Further-

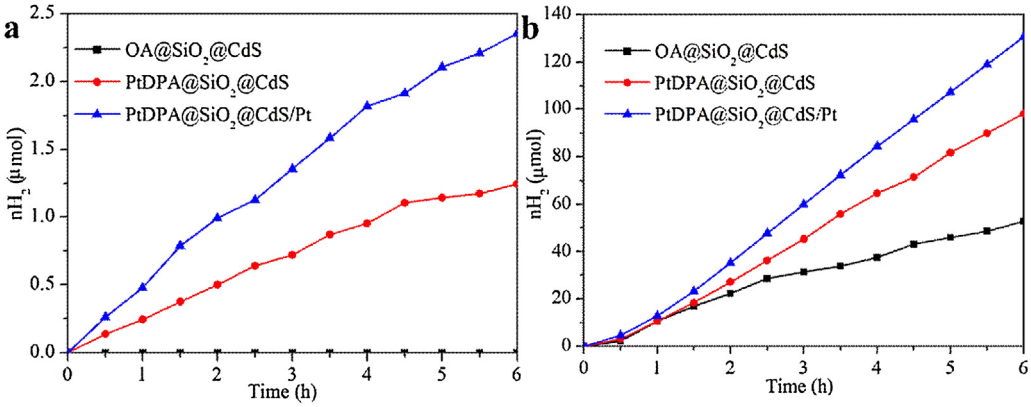

Fig. 11. (a) Under the xenon lamp radiation with a 520 nm hand-pass optical filter and (b) under the visible light irradiation, photocatalytic hydrogen evolution over OA@SiO_2@CdS, PtDPA@SiO_2@CdS and PtDPA@SiO_2@CdS/Pt.

more, an enhanced evolution of hydrogen over PtDPA@SiO_2@CdS compared with OA@SiO_2@CdS can be attributed to TTA-UCL induced activity. The utmost quantum efficiency of hydrogen evolution is observed over PtDPA@SiO_2@CdS/Pt. This simple study opens a distinctive perspective for building a kind of TTA-based upconversion–photocatalysis system.

Acknowledgements

This work was supported by the National Natural Science Foundation of China (No. 51502143), Natural Science Foundation of Jiangsu Province (No. BK20150919), Key University Science Research Project of Jiangsu Province (No. 15KJB430022), and the Startup Foundation for Introducing Talent of NUIST (2014r037), General Project of Youth Science Foundation of Jiangsu Province China (SBK2015043512), Natural Science Foundation of Jiangsu Province (No. BK20141459), Project on the Integration of Industry, Education and Research of Jiangsu Province (No. BY2015005-16, BK20150919), Qing Lan Project, Six Talent Peaks Project in Jiangsu Province (No. XCL-029) and the Project Funded by the Priority Academic Program Development of the Jiangsu Higher Education Institutions (PAPD).

Appendix A. Supplementary data

Supplementary data associated with this article can be found, in the online version, at http://dx.doi.org/10.1016/j.apcatb.2017.05.069.

References

[1] C.C. Chen, W.H. Ma, J.C. Zhao, Chem. Soc. Rev. 39 (2010) 4206–4219.
[2] W. Wang, Y.J. Zhou, Y.R. Ni, C.H. Lu, Z.Z. Xu, Mater. Lett. 145 (2015) 180–183.
[3] J.Y. Gan, X.H. Lu, Y.X. Tong, Nanoscale 6 (2014) 7142–7164.
[4] J. Liu, Y. Liu, N.Y. Liu, Y.Z. Han, X. Zhang, H. Huang, Y. Lifshitz, S.T. Lee, J. Zhong, Z.H. Kang, Science 347 (2015) 967–970.
[5] Y.N. Tang, W.H. Di, X.S. Zhai, R.Y. Yang, W.P. Qin, ACS Catal. 3 (2013) 405–412.
[6] L.T. Su, S.K. Karuturi, J.S. Luo, L.J. Liu, X.F. Liu, J. Guo, T.C. Sum, R. Deng, H.J. Fan, X.G. Liu, A.I.Y. Tok, Adv. Mater. 25 (2013) 1603–1607.
[7] W. Wang, M.Y. Ding, C.H. Lu, Y.R. Ni, Z.Z. Xu, Appl. Catal. B 144 (2014) 379–385.
[8] F. Auzel, Chem. Rev. 104 (2004) 139.
[9] G.F. Wang, Q. Peng, Y.D. Li, Acc. Chem. Res. 44 (2011) 322–332.
[10] H. Dong, L.D. Sun, C.H. Yan, Nanoscale 5 (2013) 5703–5714.
[11] T.F. Zhou, J.C. Hu, J.L. Li, Appl. Catal. B 110 (2011) 221–230.
[12] L. Ren, X. Qi, Y.D. Liu, Z.G. Huang, X.L. Wei, J. Li, L.W. Yang, J.X. Zhong, J. Mater. Chem. 22 (2012) 11765–11771.
[13] W. Wang, W.J. Huang, Y.R. Ni, C.H. Lu, Z.Z. Xu, ACS Appl. Mater. Interface 6 (2014) 340–348.
[14] X.J. Xie, N.Y. Gao, R.R. Deng, Q. Sun, Q.H. Xu, X.G. Liu, J. Am. Chem. Soc. 135 (2013) 12608–12611.
[15] X. Chen, W. Xu, L.H. Zhang, X. Bai, S.B. Cui, D.L. Zhou, Z. Yin, H.W. Song, D.H. Kim, Adv. Funct. Mater. 25 (2015) 5462–5471.
[16] M. Haase, H. Schäfer, Angew. Chem. Int. Ed. 50 (2011) 5808–5829.
[17] J.Z. Zhao, S.M. Ji, H.M. Guo, RSC Adv. 1 (2011) 937–950.
[18] P. Ceroni, Chem. Eur. J. 17 (2011) 9560–9564.
[19] F.N. Castellano, Acc. Chem. Res. 48 (2015) 828–839.
[20] H. van Eersel, P.A. Bobbert, R.A.J. Janssen, R. Coehoorn, J. Appl. Phys. 119 (2016) 163102.
[21] D.Y. Kondakov, Philos. Trans. R. Soc. A 373 (2015) 1–16.
[22] D.L. Zhou, X.J. Zheng, H.Y. Wang, J. Huang, Y.J. Luo, J. Zhou, J.S. Yu, Z.Y. Lu, Synth. Met. 220 (2016) 323–328.
[23] B. Tian, Q.H. Wang, Q.Q. Su, W. Feng, F.Y. Li, Biomaterials 112 (2017) 10–19.
[24] Q. Liu, B.R. Yin, T.S. Yang, Y.C. Yang, Z. Shen, P. Yao, F.Y. Li, J. Am. Chem. Soc. 135 (2013) 5029–5037.
[25] S.H.C. Askes, W. Pomp, S.L. Hopkins, A. Kros, S. Wu, T. Schmidt, S. Bonnet, Small 12 (2016) 5579–5590.
[26] O.S. Kwon, J.H. Kim, J.K. Cho, J.H. Kim, ACS Appl. Mater. Interfaces 7 (2015) 318–325.
[27] E.L. Cates, S.L. Chinnapongse, J.-H. Kim, J.-H. Kim, Environ. Sci. Technol. 46 (2012) 12316–12328.
[28] J.H. Kim, J.H. Kim, J. Am. Chem. Soc. 134 (2012) 17478–17481.
[29] F.F. Zhong, A. Karatay, L. Zhao, J.Z. Zhao, C. He, C.S. Zhang, H.G. Yaglioglu, A. Elmali, B. Küçüköz, M. Hayvali, Inorg. Chem. 54 (2015) 7803–7817.
[30] J.F. Sun, W.H. Wu, H.M. Guo, J.Z. Zhao, Eur. J. Inorg. Chem (2011) 3165–3173.
[31] S. Guo, W.H. Wu, H.M. Guo, J.Z. Zhao, J. Org. Chem. 77 (2012) 3933–3943.
[32] K. Tanaka, K. Inafuku, Y. Chujo, Chem. Commun. 46 (2010) 4378–4380.
[33] A. Turshatov, D. Busko, S. Baluschev, T. Miteva, K. Landfester, New J. Phys. 13 (2011) 83035.
[34] C. Wohnhaas, K. Friedemann, D. Busko, K. Landfester, S. Baluschev, D. Crespy, A. Turshatov, ACS Macro Lett. 2 (2013) 446–450.
[35] J.H. Kim, J.H. Kim, ACS Photon. 2 (2015) 633–638.
[36] D.B. Papkovsky, T.C. O'Riordan, J. Fluoresc. 15 (2005) 569–584.
[37] Q. Li, B.D. Guo, J.G. Yu, J.R. Ran, B.H. Zhang, H.J. Yan, J.R. Gong, J. Am. Chem. Soc. 133 (2011) 10878–10884.
[38] F.K. Ma, Y.Z. Wu, Y.L. Shao, Y.Y. Zhong, J.X. Lv, X.P. Hao, Nano Energy 27 (2016) 466–474.
[39] M.Q. Yang, C. Han, Y.J. Xu, J. Phys. Chem. C 119 (2015) 27234–27246.
[40] N.V. Yong, M. Ohtaki, M. Uchida, R. Jalem, H. Hirata, N.D. Chien, M. Nogami, J. Colloid Interface Sci 359 (2011) 339–350.
[41] J.J. Murcia, J.A. Navio, M.C. Hidalgo, Appl. Catal. B 126 (2012) 76–85.
[42] Y. Lei, J. Jelic, L.C. Nitsche, R. Meyer, J. Miller, Top. Catal. 54 (2011) 334–348.
[43] S. Kundu, J. Ciston, S.D. Senanayake, D.A. Arena, E. Fujita, D. Stacchiola, L. Barrio, R.M. Navarro, J.L.G. Fierro, J.A. Rodriguez, J. Phys. Chem. C 116 (2012) 14062–14070.
[44] J. Fritsche, D. Kraft, A. Thißen, T. Mayer, A. Klein, W. Jaegermann, Thin Solid Films 403–404 (2002) 252–257.
[45] J.H. Yang, H.J. Yan, X.L. Wang, F.Y. Wen, Z.J. Wang, D.Y. Fan, J.Y. Shi, C. Li, J. Catal. 290 (2012) 151–157.